



## Silver–tungsten carbide nanohybrid for efficient electrocatalysis of oxygen reduction reaction in microbial fuel cell

Xiao-Bo Gong<sup>a</sup>, Shi-Jie You<sup>a,b,\*</sup>, Xiu-Heng Wang<sup>a,\*</sup>, Yang Gan<sup>b</sup>, Rong-Ning Zhang<sup>a</sup>, Nan-Qi Ren<sup>a</sup>

<sup>a</sup> State Key Laboratory of Urban Water Resources and Environments (SKLUWRE), Harbin Institute of Technology, Harbin 150090, PR China

<sup>b</sup> Department of Catalysis Science and Engineering, School of Chemical Engineering and Technology, Harbin Institute of Technology, Harbin 150001, China

### H I G H L I G H T S

- Ag–WC/C nanohybrids are synthesized using hydrothermal method.
- Ag–WC/C nanohybrids show high-activity toward pH-neutral ORR.
- Ag–WC/C nanohybrids improve the sustainability of MFC.

### A R T I C L E I N F O

#### Article history:

Received 18 August 2012

Received in revised form

11 October 2012

Accepted 12 October 2012

Available online 29 October 2012

#### Keywords:

Silver–tungsten carbide nanohybrid

Oxygen reduction reaction

Microbial fuel cell

pH-neutral electrolyte

### A B S T R A C T

Microbial fuel cell (MFC) is able to produce electricity from organic compounds upon anodic electrochemically active microorganisms (negative electrode) and cathodic oxygen reduction reaction (ORR, positive electrode). The diminution in ORR activity associated with the pH-neutral electrolyte degrades the cathode performance of MFC. To optimize the thermodynamic process of ORR involving dissociative chemisorptions of molecular oxygen onto metal surface and subsequent electroreduction of oxides, we synthesize the carbon-supported nanometer silver/tungsten carbide hybrid (Ag–WC/C) using hydrothermal method and evaluate its electrochemical activity in pH-neutral phosphate buffer solution. Both the powder X-ray diffraction analysis and transmission electron microscopy observation suggest the formation of nanocrystalline structure of Ag (homogeneous particles of average 14 nm) and WC crystals that were uniformly dispersed on amorphous carbon support. Based on electrochemical measurements, the Ag–WC/C nanohybrids achieve catalysis of four-electron ORR with efficiency being comparable to commercial Pt/C catalyst. The promoted ORR activity should originate from the synergistic effect between WC and Ag nanoparticles. The inexpensive Ag–WC/C catalyst can produce a comparable magnitude of power density to commercial Pt/C catalyst in MFC. This study gives a demonstration of platinum-free high-efficiency and cost-effective ORR electrocatalyst for more sustainable electricity generation from biomass materials in MFC.

Crown Copyright © 2012 Published by Elsevier B.V. All rights reserved.

### 1. Introduction

With growing crisis in energy conservation and environmental pollution, a particular emphasis has been placed on sustainable conversion of environment-friendly feedstock to valuable matters and energy. Fuel cells technology provides a sustainable strategic manner for energy conversion with high-efficiency and cleanliness,

but it has to rely on simple small-molecular high energy-containing fuels such as hydrogen, methanol, formate and ethanol [1]. The high-purity fuel-processing process not only increases the complexity and operational cost, but also decreases the overall efficiency of the system [2]. To further decrease the loss of conversion efficiency and emission of greenhouse gas, it is highly expected to develop a fuel cell that is capable of directly utilizing complex organic substances (e.g. biomass) without any additional processing. Microbial fuel cell (MFC) represents a promising new fuel cell fashion to produce electricity from a diversity of organic substrates (e.g. sugar, fatty acids, proteins, and even complex wastewater [3]) through direct oxidation by electrochemical active microorganisms under ambient conditions. Unlike chemical fuel cell where strong acid or alkaline is used as electrolyte, microbial

\* Corresponding authors. State Key Laboratory of Urban Water Resources and Environments (SKLUWRE), Harbin Institute of Technology, PO Box 2603#, No. 73 Huanghe Road, Nangang District, Harbin 150090, PR China. Tel.: +86 451 86283008; fax: +86 451 86282110.

E-mail addresses: [sjyou@hit.edu.cn](mailto:sjyou@hit.edu.cn), [shijieyou@gmail.com](mailto:shijieyou@gmail.com) (S.-J. You), [xiuheng@hit.edu.cn](mailto:xiuheng@hit.edu.cn) (X.-H. Wang).

proliferation requires the electrodes to be immersed in pH-neutral solution, which leads to kinetic sluggishness of cathodic oxygen reduction and large overpotential [4].

Electrochemical reduction of dioxygen on solid electrode is a complex heterogeneous catalytic reaction involving multiple steps and several intermediate species. Depending on electrocatalyst and electrolyte used, the oxygen reduction reaction (ORR) generally takes place through two-electron or four-electron pathway, which is characterized by the reduced product of hydrogen peroxide ( $\text{H}_2\text{O}_2$ ) or water ( $\text{H}_2\text{O}$ ). For the former case,  $\text{H}_2\text{O}_2$  can be further electrochemically reduced to water, giving rise to overall indirect in-series four-electron pathway [5]. In order for MFC to maximize power density and energy conversion, four-electron ORR process is highly desirable. This makes it of particular interest to explore highly active electrocatalyst toward four-electron ORR under pH-neutral condition for MFC. However, a number of electrocatalysts (e.g. Pt [6], Pt alloy [7], CoTMPP [8], nitrogen-doped materials [9]) introduced from conventional chemical fuel cells have been tested for high-efficiency power production in MFC with limited satisfactory. One important reason for the diminution in ORR performance should be associated with the increased pH of catholyte which stems from transmembrane pH imbalance during operation as reported previously [10]. Despite the best performance of platinum catalyst observed hitherto, the high cost and scarcity of platinum constitute the stumbling block in the drive for scale-up applications. Therefore, developing low-cost and high-activity electrocatalyst toward pH-neutral ORR is essential for sustainable power production from biomass in this bioelectrochemical system.

A simplified mode describing the ORR process considers the dissociative chemisorptions of molecular oxygen (cleavage of O–O bond) onto the metal surface (the formation of M–O bond), followed by further electroreduction of the MO to water via accepting protons and electrons [11]. As is illustrated in Table 1, the metals like Ag, Au, Pd, and Hg can proceed with electroreduction of their oxides at more positive electrode potential, but the Gibbs free energy data suggest the thermodynamic unfavorable initial cleavage of O–O bond on these metals and thus less stable M–O bond. On the contrary, the metal of Zn, Mn, and V does stabilize the M–O bond more considerably (much more negative Gibbs free energy), which implies that more negative potential should be provided to accomplish the oxide electroreduction. Obviously, too negative potential means to be of less practical significance in fuel cell applications. Based on this ideology, if one could establish a metal ( $\text{M}_1$ ) that facilitates the cleavage of O–O bond, in combination with the metal  $\text{M}_2$  that favors electroreduction of its oxide ( $\text{M}_2\text{O}$ ) at relatively positive potential, the migration of oxygen atoms from  $\text{M}_1$  to  $\text{M}_2$  and thus more efficient pH-neutral ORR process would be

expected. Although it seems unlikely that the oxygen atoms migrate from one more stable oxide ( $\text{M}_1\text{O}$ ) to the other less stable oxide ( $\text{M}_2\text{O}$ ) spontaneously in macroscale system, it would be possible to realize the migration of oxygen atoms from A-top site of  $\text{M}_1$  to more stable three-fold site of  $\text{M}_2$  in nanoscale system [12].

The silver (Ag) can serve as available electrocatalyst that is active for chemical reduction of peroxide [14] and ORR [15], particularly in alkaline condition. Notwithstanding, the poor chemisorption of oxygen molecules onto bulk Ag metal is usually attributed to wide gap between the d-band and the Fermi level of low-coordinated Ag atoms, which accords well with the data presented in Table 1. Being similar as the size-dependent electrocatalytic activity observed on Pt [16] and Pd [17], Ag nanoparticle (<100 nm) can also catalyze ORR with promoted activity and selectivity due to high-surface area and quantum size effect, depending on the size of nanoparticles [18]. More importantly, the cost of silver was much lower than that of precious platinum (ca. 1:100). Taking into account of the nanoscale effect, positive-potential electroreduction (Table 1) as well as relatively low-cost, Ag nanoparticles will be primarily selected as the metal  $\text{M}_2$  in this study.

On the other hand, tungsten carbide (WC) has been widely studied as alternative catalyst in fuel cells since its metal-like (Pt) characteristics was first discovered by Levy and Boundart in 1973 [19]. They ascribed the increased catalytic reactivity of WC over W to the donation of electrons by carbon to 5d-band of tungsten, giving rise to a similar electronic structure as that of platinum. In the next decades, WC attracted extensive interest as catalyst or support material for a variety of processes such as methanol oxidation [20], nitrophenol oxidation [21], hydrogen evolution [22] as well as oxygen reduction [23]. Specifically, WC was capable of dissociating O–O bond via the reaction to form  $\text{WO}_3$  with  $\Delta G$  of  $-725.6 \text{ kJ mol}^{-1}$  [24], indicating thermodynamic spontaneity of tungsten to stabilize the W-oxide. Besides, unlike the metals Zn and V having very negative reduction potential (Table 1), the tungsten oxide can be electroreduced at higher potential condition (i.e.  $-0.090 \text{ V}$  for  $\text{WO}_3$  [25]). These natures make WC of particular suitability as  $\text{M}_1$  combining with Ag ( $\text{M}_2$ ) to produce nanohybrid. Therefore, were it feasible to produce nanoscale Ag/WC hybrid, the improved performance of ORR in MFC would be expected as result of synergistic effect between Ag and WC.

In this study, we synthesize a carbon-supported silver/tungsten carbide (Ag–WC/C) nanohybrid using hydrothermal method, and evaluate the electrocatalytic activity toward ORR in pH-neutral phosphate buffer solution. Firstly, the nanocrystalline structure of Ag–WC/C hybrid was characterized by X-ray diffraction, followed by morphological observation and element identification using transmission electron microscope (TEM). Secondly, the catalytic activities and electron-transfer number of Ag–WC/C hybrid were investigated using electrochemical methods including cyclic voltammogram (CV) scan, rotating disk electrode (RDE) measurements and electrochemistry impedance spectroscopy (EIS). Lastly, the ORR performance was assessed by measuring power density and polarization behavior of a glucose-feeding MFC containing Ag–WC/C-made cathode.

## 2. Experimental section

### 2.1. Preparation and characterization

The Ag–WC/C nanohybrid was synthesized by using simple hydrothermal method (HTM). Briefly, commercially available WC powder (1.0 g) was added to 25.0 mL solution containing 10.0 mL  $\text{H}_2\text{O}_2$  (30%, v/v) and 5.0 mL 2-propanol. Following the placement of 48 h, the carbon powder (Vulcan XC72, 1.0 g) was added to the mixture that was treated in ultrasonic bath for 30 min for

**Table 1**  
Thermodynamic data of different metals when interacting with molecular oxygen during ORR process [13].

Metal	$\text{M} + \text{O} \leftrightarrow \text{MO}^a$	$2\text{MO} + 4\text{H}^+ + 4\text{e}^- \leftrightarrow 2\text{M} + 2\text{H}_2\text{O}^b$
Ag	15.8	+1.41
Au	11.3	+0.94
Pd	−65.3	+0.49
Hg	−58.1	+0.51
Zn	−317.1	−0.82
Mn	−362.5	−1.07
V	−403.5	−1.24
WC	−725.6 <sup>c</sup>	−0.51 <sup>d</sup>

<sup>a</sup> The reactions are measured by Gibbs free energy ( $\Delta G$ ,  $\text{kJ mol}^{-1}$ ) at the standard conditions.

<sup>b</sup> The reactions are expressed by redox potentials at pH = 7.0 and 298 K (V vs standard hydrogen electrode, SHE) derived from the standard potentials under pH = 1.0 and 298 K by using Nernst equation.

<sup>c</sup> The oxide was commonly  $\text{WO}_3$ .

<sup>d</sup> The potential of  $\text{WO}_3$  reduction to W.

dispersion. After drying (12 h), the dry powders were bubbled with nitrogen gas to remove oxygen and then transferred to 80% capacity of the total volume of the closed Teflon™ vessel containers for reaction at 160 °C for 14 h. Following cooling at room temperature, the samples were washed several times with deionized water (DI water) and finally the WC/C powders were obtained after drying at 60 °C overnight. The as-prepared WC/C powders were added to AgNO<sub>3</sub> solution (WC:Ag = 1:2, w/w), and then treated by HTM again (160 °C; 14 h). After the autoclave was cooled down to room temperature naturally, the finalized products were centrifuged and washed (DI water), followed by drying in vacuum at 60 °C for 12 h. To identify the synergistic ORR activity of WC and Ag, individual WC/C and Ag/C were also prepared according to the procedures mentioned above. All the chemicals of analytical grade were used without further purification.

The powder X-ray diffraction (XRD) analysis was conducted on an X-ray diffractometer (Bruke D8 Adv., Germany) equipped with Cu K $\alpha$  source operated at a power of 40 keV  $\times$  30 mA. The diffraction data were recorded with  $2\theta$  ranging from 10° to 90° at counting time of 10 s and scanning step of 0.02°. The transmission electron microscopy (TEM) and high-resolution TEM (HRTEM) were performed on F-30ST (Tecnai, FEI, US) using high-resolution imaging and energy-dispersive X-ray spectroscopy (EDX) operated at accelerating voltage of 300 kV. For the preparation of samples before TEM observation, the as-synthesized materials were sonicated and suspended in ethanol solution followed by drop-cast onto carbon-coated copper grids, and then dried by solvent evaporation overnight at room temperature. The determination of the chemical composition of the electrocatalysts was taken by using an X-ray photoelectron spectrometer (XPS; PH1-5700 ESCA system, US) equipped with a hemispherical analyzer and an aluminum anode (monochromatic Al K $\alpha$  1486.6 eV) as source (at 12–14 kV and 10–20 mA). The system was operated under retarding model with a binding energy of 20–980 eV. The peaks for silver and tungsten element were calibrated with reference to C1s (284.6 eV).

## 2.2. Electrochemical measurements

The electrochemical measurements were carried out using dual working electrode PARSTAT (CHI700D, Chenhua Co. Ltd., China) electrochemical system at room temperature (25 °C). All the experiments were conducted in 50 mM phosphate buffer solution (PBS; pH7.2–7.8) saturated with gaseous O<sub>2</sub>. The conventional three-electrode electrochemical cell comprised a glassy-carbon working electrode (0.071 cm<sup>2</sup>), Ag/AgCl reference electrode (+0.195 V vs standard hydrogen electrode, 3.0 M KCl) and a platinum sheet counter electrode (2.25 cm<sup>2</sup>). The cyclic voltammetry (CV) scan was performed at potential in the range of –0.6–+0.6 V and scan rate of 5 mV s<sup>–1</sup>. For the electrochemistry impedance spectroscopy (EIS) analysis, a sine wave with frequency ranging from 10<sup>5</sup> to 10<sup>–2</sup> Hz on the top of bias potentials was applied. The obtained EIS data were fitted and simulated to predetermined equivalent electrical circuit and were then analyzed using ZSimpWin 3.10 software (Echem, US). The rotating disk electrode (RDE) measurement was performed on RRDE-3A apparatus (BAS Inc., Japan) by stepwise variation of rotating speed ( $\omega$ ) from 400 rpm to 3600 rpm. The Koutechy–Levich plots were derived from RDE data to calculate ORR electron-transfer number ( $n$ ) at different electrode potentials from the slope of fitting line ( $i^{-1}$  vs  $\omega^{-1/2}$ ) according to Koutechy–Levich equation

$$\frac{1}{i} = \frac{1}{i_K} + \frac{1}{i_L} \quad (1)$$

$$i_K = nFKC \quad (2)$$

$$i_L = 0.62nFAD^{2/3}\omega^{1/6}\nu^{-1/6}C \quad (3)$$

where  $i$  is the measured current (A),  $i_K$  the kinetic current (A),  $i_L$  the diffusion-limiting current (A),  $F$  the Faraday constant (96485 C mol<sup>–1</sup>),  $K$  the electron-transfer kinetic constant (mol<sup>–1</sup> s<sup>–1</sup>),  $C$  the bulk concentration of O<sub>2</sub> ( $2.2 \times 10^{-7}$  mol L<sup>–1</sup>),  $A$  the electrode area (0.071 cm<sup>2</sup>),  $D$  the diffusion constant of oxygen ( $1.7 \times 10^{-5}$  cm<sup>2</sup> s<sup>–1</sup>) and  $\nu$  the kinematic viscosity of the solution (0.01 cm<sup>2</sup> s<sup>–1</sup>).

## 2.3. Microbial fuel cell performance tests

The dual-chambered MFC, which had an architecture being quite similar to that used in our previous studies [6], contained an anode (no water-proofing carbon cloth, 7.0 cm<sup>2</sup>) and a cathode (7.0 cm<sup>2</sup>) placed on the opposite side of Plexiglas tube (28.0 mL). The MFC had an electrode distance of 4.0 cm and the two electrodes were connected with titanium wires across a constant resistor (1000  $\Omega$ ). Virginal wet-proofing-free carbon cloth together with a stainless steel mesh-made current collector was employed as the anode for colonization of electrochemically active microorganisms. The gas diffusion cathode was made from the stainless steel mesh substrate fabricated by fine Vulcan XC72 carbon powder, 20 wt.% Teflon™ binder layer and 60 wt.% Teflon™ diffusion layer according to the procedures developed by our group recently [26]. The electrocatalysts were adhered onto GDE using Nafion™ solution binder (5.0%). The MFCs were inoculated with activated sludge collected from the secondary sedimentation tank of local wastewater treatment plant. The medium solution contained (per liter of DI water) glucose (0.5 g), 50 mM phosphate buffer, NH<sub>4</sub>Cl (0.8 g), KCl (0.4 g) and trace elements.

Cell voltage generated during experiments was recorded every 10 min by using a multi-channel data acquisition system (PISO-813, ICP-DAS, Co. Ltd., Taiwan) connected to a personal computer via PCI interface. Voltage obtained was then converted to volumetric power density ( $P$ , W m<sup>–3</sup>) according to  $P = V^2/(R_{EX}V_{anode})$ , where  $V$  (V) is the voltage across given external resistor ( $\Omega$ ) and  $V_{anode}$  (m<sup>3</sup>) the anode volume. Polarization and power curves were obtained via recording peak stable cell voltage produced across different external resistances. The electrode potentials were recorded versus Ag/AgCl reference.

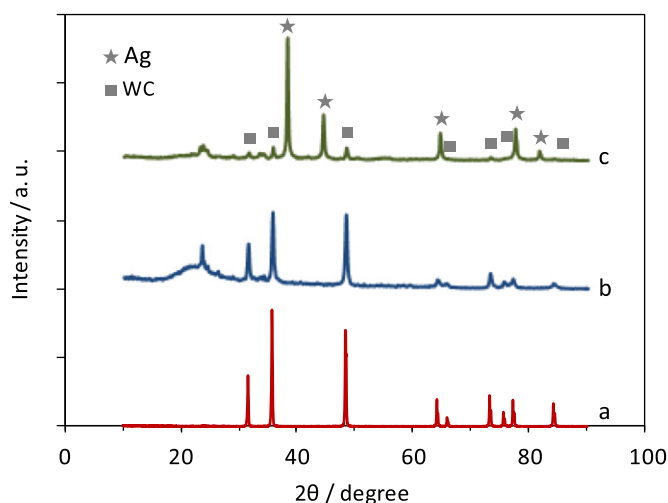
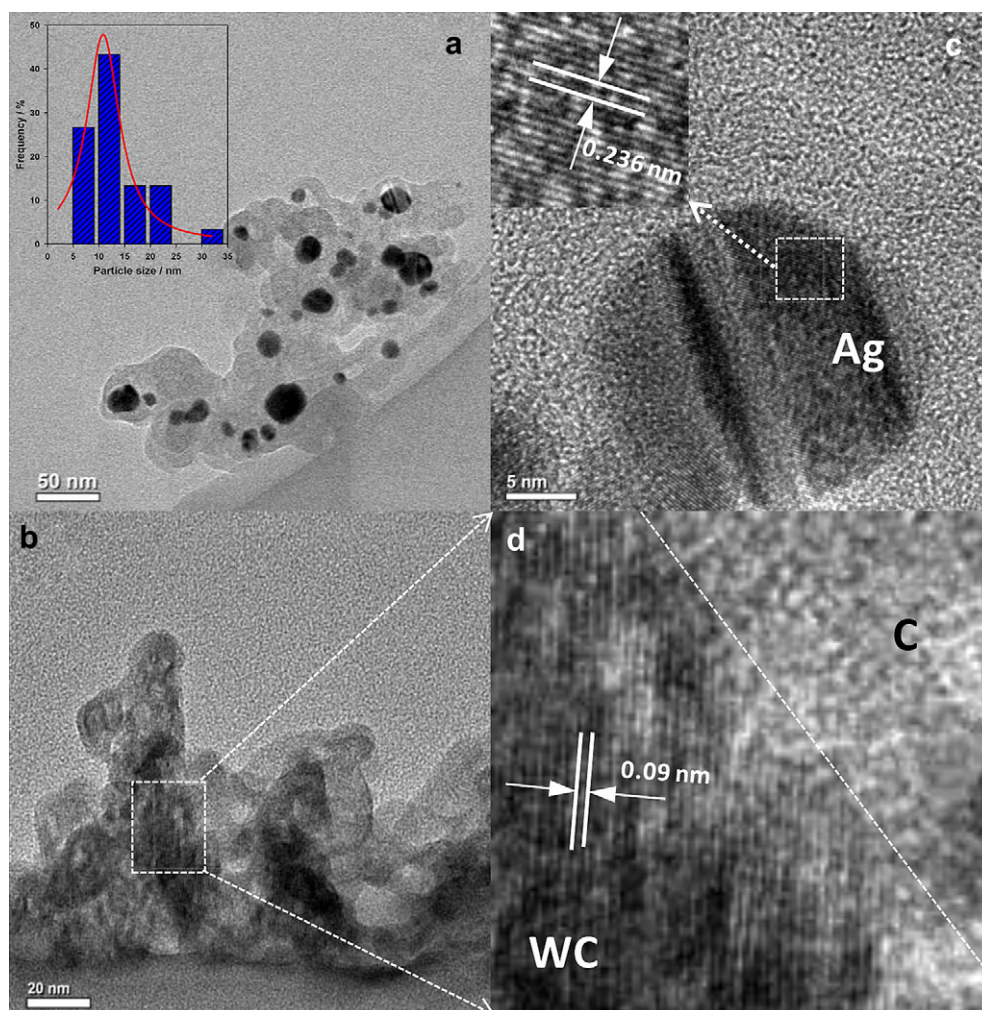
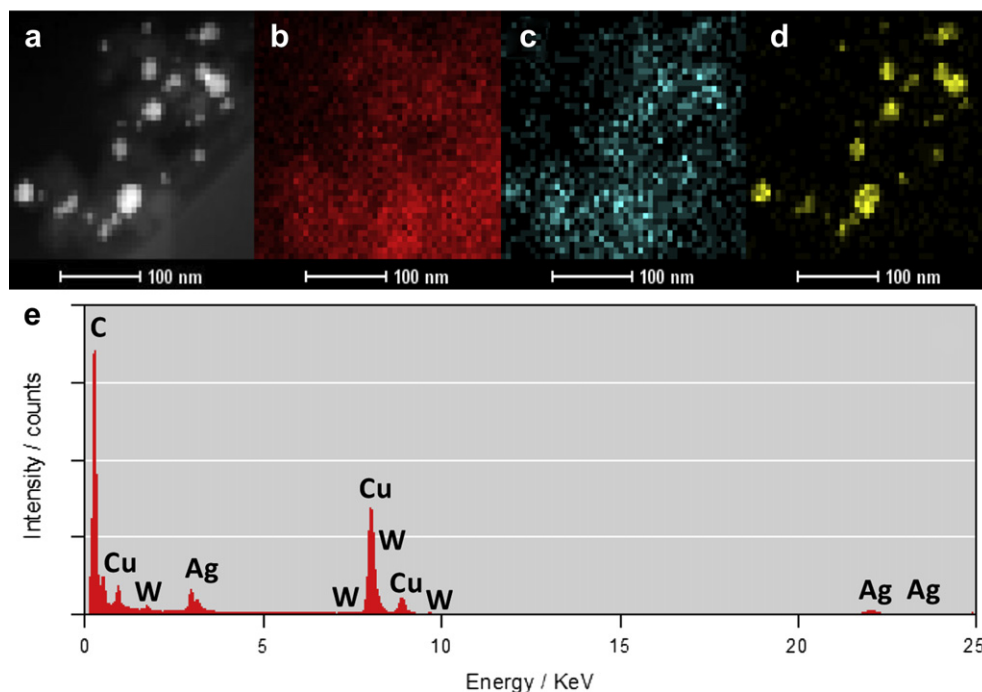


Fig. 1. XRD patterns of (a) pristine WC, (b) WC/C and (c) Ag–WC/C nanohybrid.



**Fig. 2.** (a) TEM images of as-prepared (a) Ag–WC/C and (b) WC/C samples, and HRTEM images of (c) Ag–WC/C and (d) WC/C. The inserted figure in (a) shows the particle size distribution of Ag in Ag–WC/C nanohybrid.



**Fig. 3.** HAADF-STEM images and X-ray mapping of (a) Ag–WC/C, (b) C, (c) W, (d) Ag and corresponding (e) EDX spectrum of the Ag–WC/C nanohybrid.

### 3. Results and discussion

Following the synthesis of Ag–WC/C electrocatalysts, the crystalline structure was examined using powder X-ray diffraction (XRD). Fig. 1 shows the  $2\theta$  of  $38.18^\circ$ ,  $44.36^\circ$ ,  $64.50^\circ$  and  $77.46^\circ$  with  $d$ -values of 2.3552, 2.0403, 1.4435 and 1.2311, in accordance with the (111), (200), (220) and (311) planes for Ag nanoparticles. The characteristic peaks of both WC and Ag could be clearly identified from the XRD patterns, indicating the co-existence of WC and Ag in the hybrid. The TEM observation reveals the microstructure of faceted nanocrystalline Ag (Fig. 2a and b) dispersed on WC/C supports consisting of well-defined WC crystals and amorphous carbon (Fig. 2c and d). Both TEM image (Fig. 2a) and particle size distribution figure (inserted figure in Fig. 1a) show that the discrete Ag nanoparticles had fairly uniform crystal size in diameter over the range of 8–26 nm, which was inline with the average crystal size of 14 nm calculated using Scherer equation. The high-angle annular dark-field scanning transmission electron microscopy

(HAADF-STEM, Fig. 3) clearly illustrates the overlapping zone of C and W elements where Ag was deposited homogeneously without agglomeration. The red region out of the overlapping zone accounted for carbon support existing in the gaps surrounding WC. The chemical distribution seen from HAADF-STEM accorded well with the EDX spectra (Fig. 3e). The XPS spectra indicates the incorporation of Ag into Ag–WC/C and the presence of O involved in oxygen-containing functional groups on carbon support in both Ag–WC/C and WC/C (Fig. 4). The W-oxide peaks were not identified from the XPS spectra, implying the chemical stability of WC during hydrothermal preparation. All these results confirmed the co-existence and combined crystalline structure of Ag and WC on carbon support in the hybrid.

To evaluate the ORR electrocatalytic activity, the thin films of electrocatalyst materials (WC, WC/C, Ag/C and Ag–WC/C) were immobilized onto glassy-carbon electrode for cyclic voltammogram (CV) tests in 50 mM phosphate buffer solution (PBS) saturated with  $O_2$ . For comparison, commercial Pt/C catalyst (10%) was also examined under the same conditions. Within the electrode potential varying in the range of  $-0.6$ – $+0.6$  V vs Ag/AgCl, pristine WC showed a minimal catalytic activity for ORR as indicated by extremely weak current response. The oxygen reduction current was increased when WC was loaded onto carbon support (WC/C), suggesting the importance of large surface area, conductivity and functional groups (Fig. 4) on carbon material [27]. As can be seen from Fig. 5, the pristine WC was reported to be inactive toward ORR in  $H_2SO_4$  solution due to strong oxygen bonding energy on WC [23]. However, apparent ORR activity was detected on WC/C material in PBS electrolyte, which was consistent with the observation of ORR activity on WC nanocrystal [28] and nanowire [29] in alkaline solution. Thus, it should be possible to realize ORR on WC nanocrystal resulting from large surface area for splitting of O–O bond. Remarkably, the chemical incorporation of Ag nanoparticles into WC/C resulted in a significantly increased cathodic current of 0.033 mA, a value higher than both individual WC/C and Ag/C, and close to Pt/C (0.036 mA), indicating the synergistic ORR electrocatalytic activity of Ag and WC in the nanohybrid. It was noticed that the positive scan produced an anodic peak at potential of 0.17 V and negative scan gave a cathodic peak at potential of  $-0.21$  V, which should come from chemically reversible reaction of Ag

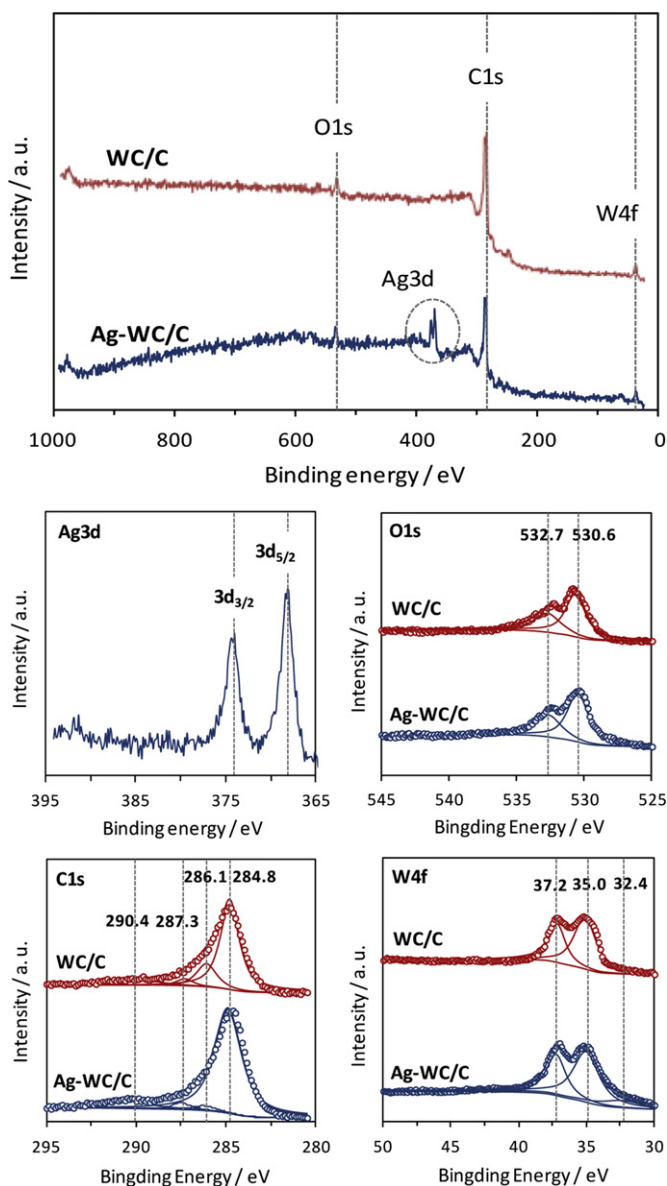


Fig. 4. XPS spectrum of Ag–WC/C and WC/C, and corresponding high-resolution Ag3d, O1s, C1s and W4f spectrum.

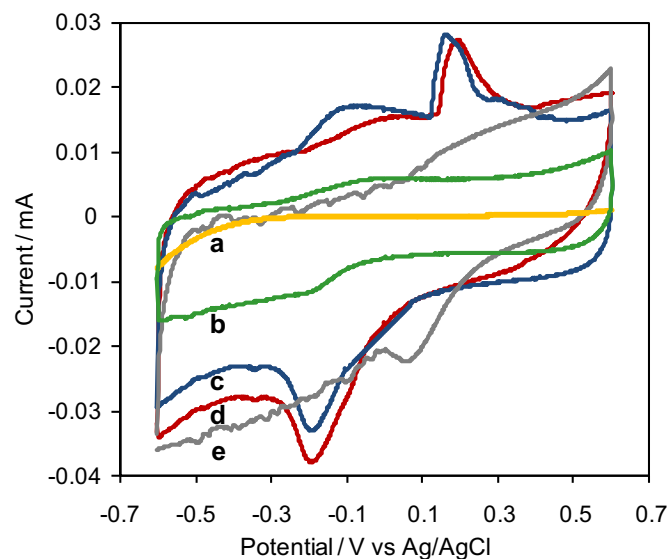


Fig. 5. Cyclic voltammograms (CVs) for ORR on (a) pristine WC, (b) WC/C, (c) Ag/C, (d) Ag–WC/C and (e) Pt/C measured in pH-neutral solution at scan rate of  $5 \text{ mV s}^{-1}$ .

nanoparticles and cationic  $\text{Ag}^+$  ( $\text{Ag}_2\text{O}$  or  $\text{AgOH}$ ), in consistence with the observation in recent studies [30]. This process should not have substantially negative impact to ORR because of good chemical reversibility indicated by the symmetric anodic and cathodic waves in voltammogram obtained under pH-neutral electrolyte.

To examine the ORR kinetics and electron-transfer number of the electrocatalysts, rotating disk electrode (RDE) tests were carried out in 50 mM  $\text{O}_2$ -saturated PBS through stepwise change of rotating rate (100–3600 rpm), and the results were given in Fig. 6a–e. The linear Koutechy–Levich plots derived from RDE data indicated the first-order ORR kinetics with respect to dissolved oxygen concentration at different electrode potentials (Fig. S1 in Supporting information). Based on the fitting lines of Koutechy–Levich plots (Fig. 6f), the overall electron-transfer number ( $n$ ) was determined to be 3.86 for ORR on Ag–WC/C nanohybrid (pH = 7.6), which was indicative of mainly four-electron oxygen reduction, approaching that on Pt/C catalyst ( $n = 3.91$ ). Notably, the Ag-free WC and WC/C

exhibited much poorer ORR activity with  $n = 2.23$  and  $n = 2.80$ , respectively, suggesting predominance of two-electron oxygen reduction on WC. The Ag/C catalyst afforded ORR ( $n = 3.1$ ) better than WC and WC/C due to appreciable ORR catalytic activity of nanometer Ag particles [15], but worse than Ag–WC/C. The results obtained from RDE measurements were in agreement with that observed in CVs scan, confirming the synergistic effect of Ag and WC for improved ORR activity in pH-neutral electrolyte. The improved ORR performance could also be verified by electrochemistry impedance spectroscopy (EIS) analysis (Fig. 7), which demonstrated smaller charge-transfer resistance (151.1  $\Omega$ ) of Ag–WC/C (0.7% greater than that of Pt/C, 146.7  $\Omega$ ) than that of Ag/C (168.2  $\Omega$ ), WC/C (174.9  $\Omega$ ) and WC (235.3  $\Omega$ ). The identical ohmic resistance (15.4  $\Omega$ ) for different catalysts was the consequence of the same PBS electrolyte used during the experiments.

The oxygen reduction on catalyst has been known a structure-sensitive and size-dependent reaction [16–18]. The remarkable

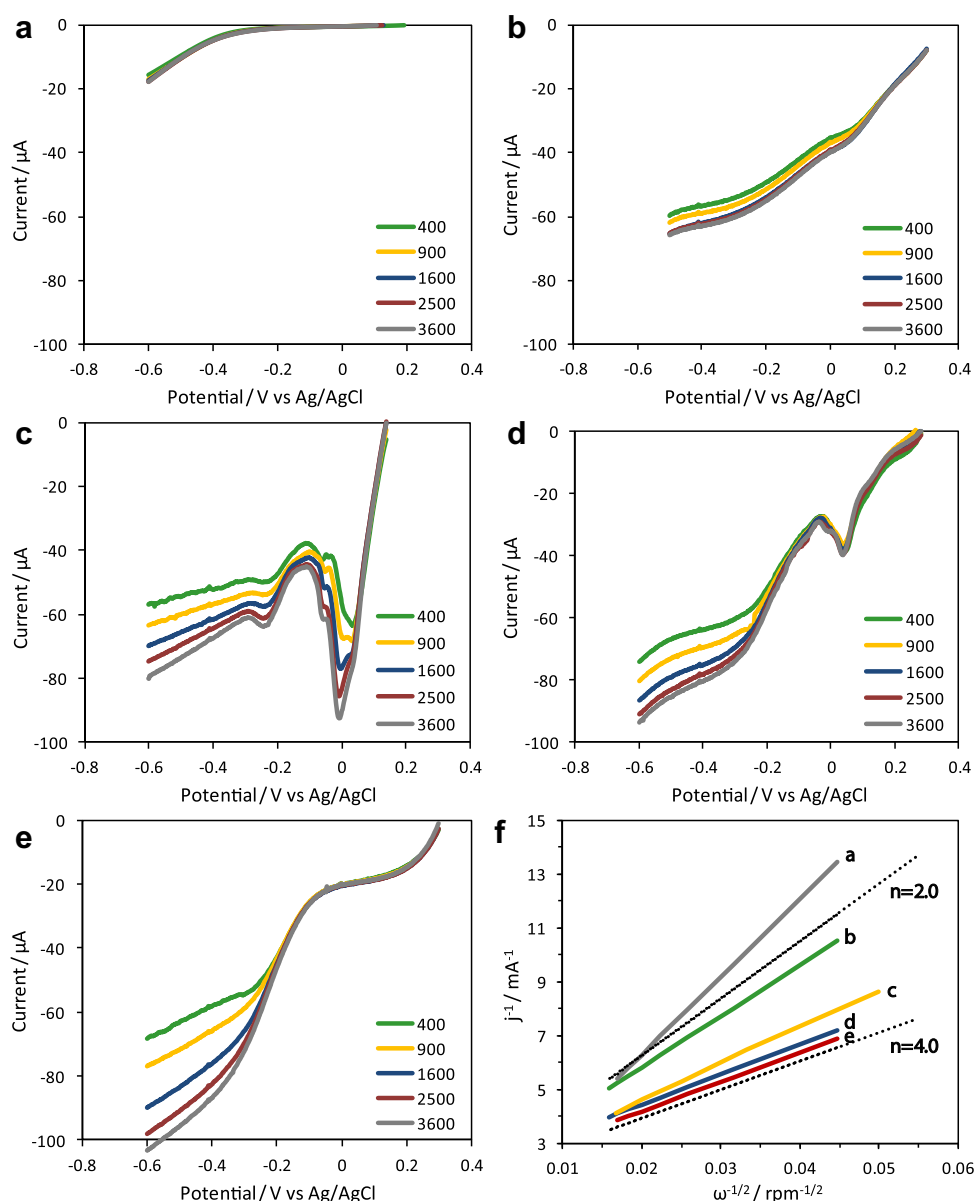


**Fig. 6.** Rotating disk voltammograms of (a) WC, (b) WC/C, (c) Ag/C, (d) Ag–WC/C and (e) Pt/C catalysts measured in  $\text{O}_2$ -saturated pH-neutral solution. (f) Koutechy–Levich plot of different electrocatalysts.

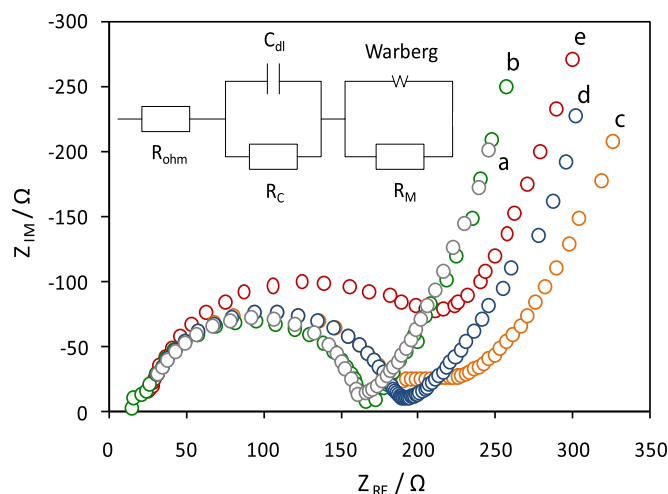


**Fig. 7.** Nyquist plots of impedance spectra of (a) pristine WC, (b) WC/C, (c) Ag/C, (d) Ag-WC/C and (e) Pt/C measured in pH-neutral solution. The inserted figure shows equivalent circuit for the electrochemical system where the symbols represent the elements of ohmic resistance ( $R_{ohm}$ ), charge-transfer resistance ( $R_c$ ), mass-transfer resistance ( $R_M$ ), double-layer capacitance ( $C_{dl}$ ) and Warburg impedance ( $W$ ).

electrocatalytic activity of Ag-WC/C nanohybrid obtained herein should be attributed to the synergistic effect of C, WC and Ag nanoparticles. The carbon powder after hydrothermal process can establish good conductive support with large surface area and oxygen-containing functional groups, e.g.  $-\text{COO}^-$ ,  $\text{C}-\text{OH}$ ,  $\text{C}=\text{O}$  as shown by the C1s and O1s peaks of XPS spectrum in Fig. 4, for the nucleation and attachment of WC and Ag nanoparticles [31]. According to the thermodynamic scheme of heterogeneous ORR, the WC tends to favor dissociate chemisorptions of O–O bond in oxygen molecule to stabilize the oxygen atom in W–O bond (e.g.  $\text{WO}_3$ ,  $\Delta G$  of  $-725.6 \text{ kJ mol}^{-1}$ ). Within the Ag-WC nanohybrid system, the oxygen atom involved in W–O bond has access to migration onto the three-fold site of Ag followed by being electroreduced to accomplish overall ORR process. The size of Ag nanoparticles (average 14 nm in diameter) obtained here was much smaller than those of size 100 nm [32,33] and 20 nm [34] synthesized previously, which facilitated migration of oxygen atom between WC and Ag, and provided large surface area and active site for heterogeneous ORR catalysis. In addition, Ag(111) nanocrystal (lattice spacing of 2.36 Å, Fig. 2c) had the most stable surface structure for complete oxygen reduction as a result of intermediate oxygen binding energy on Ag(111) facet. All these factors render the overall oxygen reduction tend to proceed in four-electron pathway on Ag-WC/C nanohybrid. On the other hand, WC/C was active for the electrocatalysis of two-electron ORR as indicated by CVs (Fig. 5) and RDE data (Fig. 6f). This was consistent with Zhou et al. [29], who reported that the pristine WC without high-temperature  $\text{NH}_3$  etching underwent mainly two-electron ORR ( $n = 2.3$ ) route, which led to WC oxidation by peroxide species in alkaline solution. Here, owing to the excellent catalytic activity of Ag, the absorbed peroxide produced on WC could be rapidly reduced or decomposed to form water [14,35]. This might also result in indirect “ $\text{O}_2\text{--H}_2\text{O}_2\text{--H}_2\text{O}$ ” four-electron ORR pathway on Ag-WC/C nanohybrid.

The electrocatalytic stability of Ag-WC/C nanohybrid was investigated by recording normalized ORR current versus electrode potential for 100 cycles. Fig. 8 shows that the decrease in normalized ORR current of the Ag-WC/C (by 21.6%) was only slightly greater than that of Pt/C (by 20.2%) after 100-cycle CV scan, indicating similar durability of both electrocatalysts. Several reasons may cause activity loss of the electrocatalyst. For the Pt/C, the detachment and agglomeration of Pt particles together with

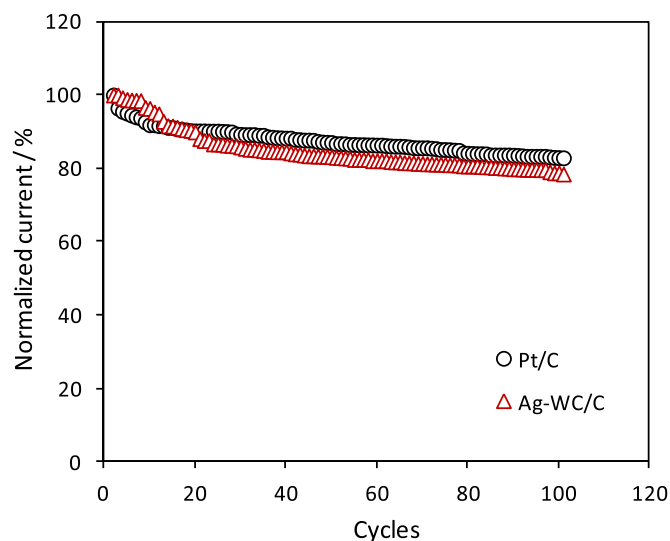


**Fig. 8.** Comparison of electrochemical durability of Pt/C and Ag-WC/C electrocatalyst for ORR in pH-neutral solution.

Ostwald ripening may cause substantial decrease in electrochemical surface area (ECSA) and activity [36]. These factors can also apply to explain the activity loss of Ag-WC/C catalyst. Another possible reason for activity loss could be that in the pH-neutral PBS solution, phosphate (i.e.  $\text{HPO}_4^{2-}$ ,  $\text{H}_2\text{PO}_4^-$ ,  $\text{PO}_4^{3-}$ ) may adsorb onto the catalyst, blocking part of active surface area and changing Gibbs free energy of ORR intermediate adsorption. This mechanism is similar to the impact of  $\text{OH}^-$  on the catalytic ORR in alkaline fuel cell [37]. In particular, the  $\text{Ag}^+$  produced from oxidation of Ag nanoparticles may partially combine with phosphate to form  $\text{Ag}_3\text{PO}_4$  deposition, whereby the ECSA was reduced on Ag-WC/C hybrid. In addition, the W-oxides (i.e.  $\text{WO}_2$ ,  $\text{WO}_3$ ) resulting from the O–O bond splitting and hydrolysis of WC could undergo aqueous dissolution to form soluble complex such as  $\text{H}_3\text{W}_6\text{O}_{21}^{3-}$  (dissolution constant of  $1.3 \times 10^{-7} \text{ mol m}^{-2} \text{ h}^{-1}$ ) [38]. This might also be responsible for activity diminution of the Ag-WC/C hybrid during ORR.

To perform further assessment on the availability of Ag-WC/C nanohybrid for ORR in pH-neutral solution, we attached the electrocatalysts (the identical loading of  $6.43 \text{ mg cm}^{-2}$ ) onto the surface of Teflon<sup>TM</sup>-treated gas diffusion electrode (GDE), and applied this as-prepared GDE to the air-breathing cathode of dual-chamber PBS-containing (50.0 mM) microbial fuel cell (MFC). Hydrophilic Nafion<sup>TM</sup> ionomer (5%) was used as binder solution to improve the three-phase interfacial contact between oxygen (air), aqueous electrolyte and electrocatalyst. The batch-fed operation gave rise to different reproducible cell voltages (constant external resistance of  $1000 \Omega$ ) depending on the cathodic catalyst used, as expected, which followed order of  $\text{Pt/C} > \text{Ag-WC/C} > \text{Ag/C} > \text{WC/C} > \text{WC}$  (Fig. S2 in Supporting information) during each reaction cycle. Based on the measurements of resistance-dependent current density and electrode potential versus Ag/AgCl, the polarization and power density curves were obtained. The electrode polarization curves (Fig. 9a) show the predominance of cathode potential and indifference in variation of anode potential with regard to electrocatalyst, suggesting the power output of MFC was primarily governed by the cathodic ORR performance. With the synergistic effects of WC and Ag, the Ag-WC/C nanohybrid exhibited good ORR activity in terms of comparable potential and overpotential to the Pt/C catalyst. Accordingly, the maximum volumetric power density of  $20.62 \text{ W m}^{-3}$  using Ag-WC/C nearly approached that of  $21.40 \text{ W m}^{-3}$  using Pt/C catalyst (Fig. 9b). These results clearly

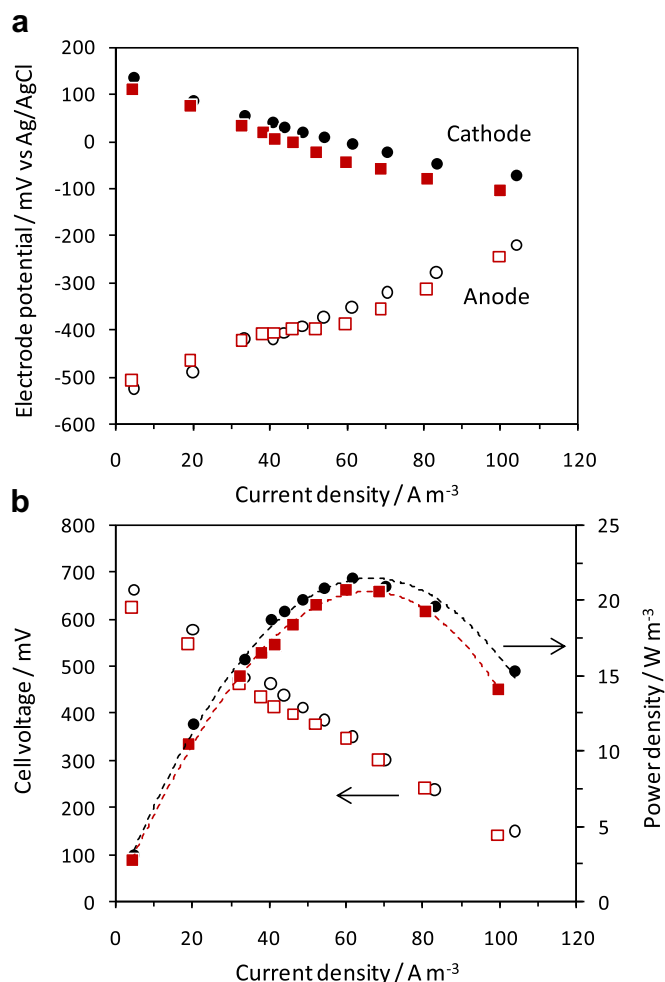


**Fig. 9.** (a) Electrode potential and (b) cell voltage and volumetric power density as function of current density in the MFC with the cathode made from Ag–WC/C nanohybrid (square symbols) and Pt/C (circle symbols) electrocatalyst.

indicated that the Ag–WC/C nanohybrid could be used a good alternative to conventional Pt/C catalyst for cost-effective electricity production without losing power efficiency and stability.

#### 4. Conclusions

In conclusion, based on thermodynamic principle of oxygen bond splitting and adsorbed oxygen electroreduction, Ag and WC were selected to fabricate nanohybrid catalyst to improve the ORR in pH-neutral electrolyte. As indicated by CVs, RDE and EIS measurements, the hydrothermally synthesized Ag–WC/C nanohybrid was shown highly active for electrocatalysis of oxygen reduction in pH-neutral electrolyte. With the nanometers-scale synergistic effects of carbon, tungsten carbide and silver nanoparticles, the ORR on Ag–WC/C nanohybrid could take place through the overall four-electron pathway. By virtue of considerably lower cost of Ag (1/100th the price of Pt) and WC material, the Ag–WC/C-cathode MFC could generate electricity from glucose substrate much more economically and sustainably over Pt/C-cathode MFC. This study not only provides a simple approach to making the platinum-free Ag–WC/C nanohybrid for efficient electrocatalysis of oxygen reduction in MFC, but also suggests promising potential for this nanoelectrocatalyst to be used for other

pH-neutral electrolyte processes such as hydrogen evolution in microbial electrolysis and water oxidation in oxygen electrolysis reaction.

#### Acknowledgements

Project supported by the National Natural Science Foundation of China (Grant Nos. 51108121, 51178140), State Key Laboratory of Urban Water Resource and Environment (Grant No. 2012DX05), and the Project 51121062 (National Creative Research Groups) supported by National Nature Science Foundation of China.

#### Appendix A. Supplementary data

Supplementary data related to this article can be found at <http://dx.doi.org/10.1016/j.jpowsour.2012.10.047>.

#### References

- [1] W. Vielstich, A. Lamm, H.A. Gasteiger, *Handbook of Fuel Cells – Fundamentals, Technology and Applications*, John Wiley & Sons, Chichester, 2003.
- [2] B.C.H. Steele, A. Heinzel, *Nature* 414 (2001) 345–352.
- [3] D. Pant, G. van Bogaert, L. Diels, K. Vanbroekhoven, *Bioresour. Technol.* 101 (2010) 1533–1543.
- [4] F. Harnisch, U. Schröder, *Chem. Soc. Rev.* 39 (2010) 4433–4448.
- [5] K. Kinoshita, *Electrochemical Oxygen Technology*, John Wiley & Sons, New York, 1992.
- [6] S. Cheng, H. Liu, B.E. Logan, *Electrochem. Commun.* 8 (2006) 489–494.
- [7] J.N. Zhang, S.J. You, Y.X. Yuan, Q.L. Zhao, G.D. Zhang, *Electrochem. Commun.* 13 (2011) 903–905.
- [8] F. Zhao, F. Harnisch, U. Schröder, F. Scholz, P. Bogdanoff, I. Herrmann, *Electrochem. Commun.* 7 (2005) 1405–1410.
- [9] L. Feng, Y. Chen, L. Chen, *ACS Nano* 5 (2011) 9611–9618.
- [10] F. Zhao, F. Harnisch, U. Schröder, F. Scholz, P. Bogdanoff, I. Herrmann, *Environ. Sci. Technol.* 40 (2006) 5193–5199.
- [11] J.L. Fernández, D.A. Walsh, A.J. Bard, *J. Am. Chem. Soc.* 127 (2005) 357–365.
- [12] Y. Xu, A.V. Ruban, M. Mavrikakis, *J. Am. Chem. Soc.* 126 (2004) 4717–4725.
- [13] A.J. Bard, R. Parsons, J. Jordan (Eds.), *Marcel Dekker*, New York, 1985.
- [14] F.W. Campbell, S.R. Belding, R. Baron, L. Xiao, R.G. Compton, *J. Phys. Chem. C* 113 (2009) 9053–9062.
- [15] H. Bunazawa, Y. Yamazaki, *J. Power Sources* 182 (2008) 48–51.
- [16] N.G. Shang, P. Papakonstantinou, P. Wang, S.R.P. Silva, *J. Phys. Chem. C* 114 (2010) 15837–15841.
- [17] W. Tang, H.F. Lin, A. Kleiman-Shwarsztajn, G.D. Stucky, E.W. McFarland, *J. Phys. Chem. C* 112 (2008) 10515–10519.
- [18] Y. Lu, W. Chen, *J. Power Sources* 197 (2012) 107–110.
- [19] R.B. Levy, M. Boudart, *Science* 181 (1973) 547–549.
- [20] R. Ganesan, J.S. Lee, *Angew. Chem. Int. Ed.* 44 (2005) 6557–6560.
- [21] G.H. Li, C.A. Ma, Y.F. Zheng, W.M. Zhang, *Micropor. Mesopor. Mater.* 85 (2005) 234–240.
- [22] L. Schlapbach, A. Züttel, *Nature* 414 (2001) 353–358.
- [23] I.J. Hsu, D.A. Hansgen, B.E. McCandless, B.G. Willis, J.G. Chen, *J. Phys. Chem. C* 115 (2011) 3709–3715.
- [24] A. Warren, A. Nylund, I. Olefjord, *Int. J. Refract. Met. Hard Mater.* 14 (1996) 345–353.
- [25] G. Milazzo, S. Garoli, V.K. Sharma, *Tables of Standard Electrode Potentials*, Wiley, Chichester, 1978.
- [26] S.J. You, X.H. Wang, J.N. Zhang, J.Y. Wang, N.Q. Ren, X.B. Gong, *Biosens. Bioelectron.* 26 (2011) 2142–2146.
- [27] Y. Liang, Y. Li, H. Wang, J. Zhou, J. Wang, T. Regier, H. Dai, *Nat. Mater.* 10 (2011) 780–786.
- [28] H. Meng, P.K. Shen, *Chem. Commun.* 35 (2005) 4408–4410.
- [29] X. Zhou, Y. Qiu, J. Yu, J. Yin, S. Gao, *Int. J. Hydrogen Energ* 36 (2011) 7398–7404.
- [30] M. Giovanni, M. Pumera, *Electroanal.* 64 (2012) 615–617.
- [31] Z.P. Zhu, D.S. Su, G. Weinberg, R. Schlögl, *Nano Lett.* 4 (2004) 2255–2259.
- [32] G.K.H. Wiberg, K.J.J. Mayrhofer, M. Arenz, *Fuel Cells* 10 (2010) 575–581.
- [33] J. An, H. Jeon, J. Lee, I.S. Chang, *Environ. Sci. Technol.* 45 (2011) 5441–5446.
- [34] Y. Yang, Y. Zhou, *J. Electroanal. Chem.* 397 (1995) 271–278.
- [35] J.S. Spendlow, A. Wieckowski, *Phys. Chem. Chem. Phys.* 9 (2007) 2654–2675.
- [36] H.W. Liang, X. Cao, F. Zhou, C.H. Cui, W.J. Zhang, S.H. Yu, *Adv. Mater.* 23 (2011) 1467–1471.
- [37] N.R. Elezovic, B.M. Babic, Li. Gajic-Krstajic, P. Ercius, V.R. Radmilovic, N.V. Krstajic, Li. M. Vracar, *Electrochim. Acta* 69 (2012) 239–246.
- [38] R. Ganesan, D.J. Ham, J.S. Lee, *Electrochem. Commun.* 9 (2007) 2576–2579.